Steel and Composite Structures, *Vol. 16, No. 5 (2014) 533-557*
DOI: http://dx.doi.org/10.12989/scs.2014.16.5.533

Seismic behavior of special moment-resisting frames with energy dissipating devices under near source ground motions

Mahmoud Bayat [*1] and Mahdi Bayat [2]

[1] *Young Researchers and Elites club, Science and Research Branch, Islamic Azad University, Tehran, Iran*
[2] *Young Researchers and Elites Club, Mashhad Branch, Islamic Azad University, Mashhad, Iran*

(*Received February 10, 2014, Revised February 26, 2014, Accepted March 02, 2014*)

Abstract. In this study, the performances of the SMRF building equipped with energy dissipating devices are studied. Three types of these structures with different heights are considered. The Added Damping and Stiffness (ADAS) devices are used as energy dissipating devices in these structures. The behavior of these structures with ADAS devices subjected to near source ground motions are investigated. Three SMRF buildings with five, ten and fifteen-story, with ADAS devices were chosen. The nonlinear time history analysis was used by applying the near source ground motions with PERFORM 3D.V4 and conclusions are drawn upon an energy criterion. The effect of PGA variation and height of the frames are also considered based on the energy criterion.

Keywords: Yielding Dampers (ADAS); SMRF frame; energy dissipation devices; near source ground motion

1. Introduction

Many studies have been done on the experimental analysis of metallic dampers in structures. The first study was done by Kelly *et al*. (1972) and Skinner *et al*. (1975). Kelly *et al*. (1972) proposed the idea of using metallic dampers for dissipating the seismic energy in a structural system. The authors continued the work on this type of damper by considering different deformations of steel. The focus of those studies was experimental and some analytic relations were developed to quantity the behavior of the dampers.

Aguirre and Sánchez (1992) studied the U type of dampers. They considered the Force-deformation response and the environment temperature of the sample under the load cycling in their experiment. Different shapes of low-yield metals have been used as dissipating devices. Among of them, the added damping and stiffness device (ADAS) and variations such as the TADAS (Bergman and Goel 1987, Whittaker *et al*. 1989) and Honeycomb damper have become more popular than the others (Whittaker *et al*. 1991). The energy dissipating devices have the following advantages.

(1) They can control the seismic response of a structure by using their stable and sufficient large dissipation capacity.

*Corresponding author, Researcher, E-mail: mbayat14@yahoo.com

http://www.techno-press.org/?journal=scs&subpage=8 ISSN: 1229-9367 (Print), 1598-6233 (Online)

(2) They have a representative model of its cyclic behavior.

The first usage of ADAS devices was in Mexico City (Martinez-Romero 1993). Three buildings retrofitted with ADAS elements. They used load-deformation curves obtained experimentally by the supplier of the ADAS device hardware (Whittaker *et al*. 1991). An analytical procedure was presented by Whittaker *et al*. to obtain the load-deformation curves. Pong *et al*. (2009) proposed a new procedure for designing ADAS devices and applied it to different cases. The behavior of structures is different when subjected to near-fault ground motion. Near-fault ground motions have a high level of PGA and a large vertical ground motion with an intense long-period velocity pulse wave. The intense long-period velocity pulse wave usually occurs in the beginning of a near-fault earthquake. The range of the pulse periods is from 1.4 s to 7 s for a range of earthquake magnitudes from 6 to 7.6 M based on the Baker (2007) findings. More information can be obtained by considering these useful references (Bayat and Abdollahzadeh 2011a, b, Shih and Sung 2005, Longo *et al*. 2012a, b, Ponzo *et al*. 2012, Rai *et al*. 2013, Parulekar *et al*. 2009, Apostolakis and Dargush 2010, Barrón and Ayala 2013, Constantinou and Symans 1993, Brown *et al*. 2001, Moreschi 2000, Symans *et al*. 2008, Erfani *et al*. 2014, Zahrai and Jalali 2014, Reye-Salazar *et al*. 2012). Therefore, it is very important to consider the above near-fault earthquake characteristics in the design of structures located in near-fault regions. In this study, we improve the seismic behavior of SMRF buildings with energy dissipating devices (ADAS) and analyze them under the near-fault ground motion based on energy concepts. The amount of dissipated energy in the ADAS elements is very large for different earthquake records in all cases. Fig. 1 represents the arrangement of ADAS devices.

2. Overview of input energy to a structure

The governing equation of a viscous damped SDOF system subject to horizontal earthquake ground motion is (Bayat *et al*. 2011a)

$$m\ddot{u}_t + c\dot{u} + f_S = 0 \tag{2.1}$$

If we choose $\ddot{u}_t = \ddot{u} + \ddot{u}_g$ absolute (total) displacement of mass, The Eq. (2.1) can be written as

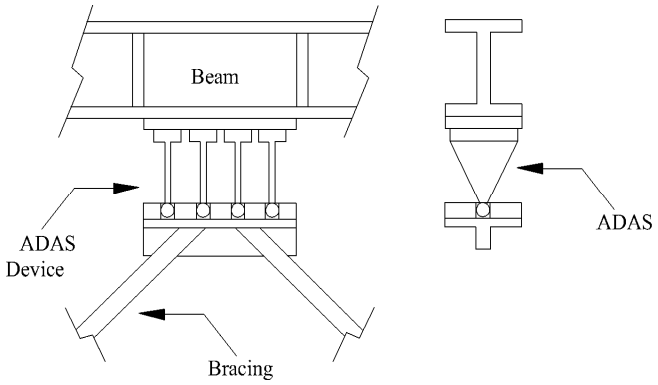

Fig. 1 Arrangement of ADAS devices (Pong *et al*. 2009)

$$m\ddot{u}_t + c\dot{u} + f_S = m\ddot{u}_g \tag{2.2}$$

An energy representation of the Eq. (2.1) can be obtained by integrating it over the entire relative displacement u

$$\int m\ddot{u}du + \int c\dot{u}du + \int f_s du = -\int m\ddot{u}_g du \tag{2.3}$$

We achieve these kinds of energies (Bayat *et al*. 2011a)

$$E_I = E_k + E_D + E_A \tag{2.4}$$

The Eq. (2.4) is the **"**Relative" Energy Equation (Bayat *et al*. 2011a).

The "relative" energy method is considered in this study to obtain the input energy of structures.

For a fixed E_I,it is better to increase the E_H then the elastic strain energy in the structure becomes minimized.

3. Designing of ADAS devices

The ADAS devices bearable forces are given as (Bayat *et al*. 2011a, Pong *et al*. 2009)

$$F_R = K'\delta_y + aK'(\delta_R - \delta_y), \tag{3.1}$$

We used a bilinear load-deformation curve in shear of the ADAS dampers can be idealized with strain hardening (Pong *et al*. 2009)

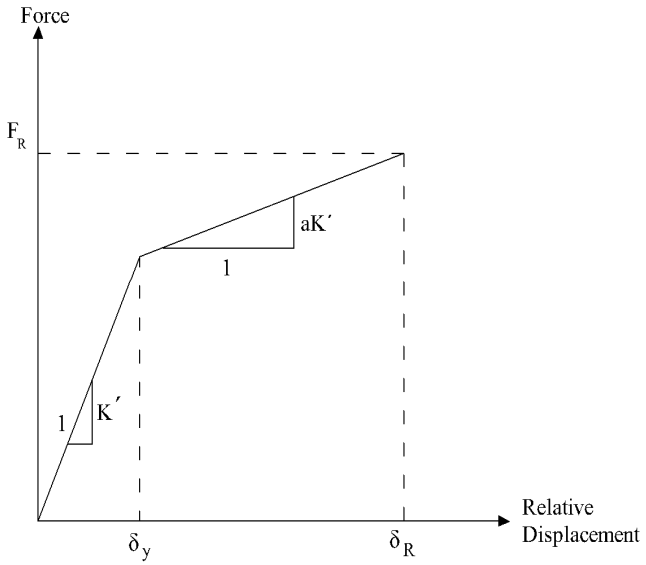

Fig. 2 The relationship between force and relative displacement of ADAS (Pong *et al*. 2009)

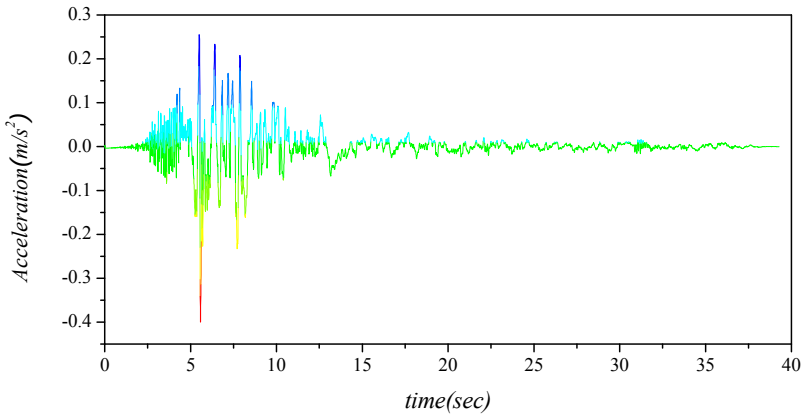

(a)

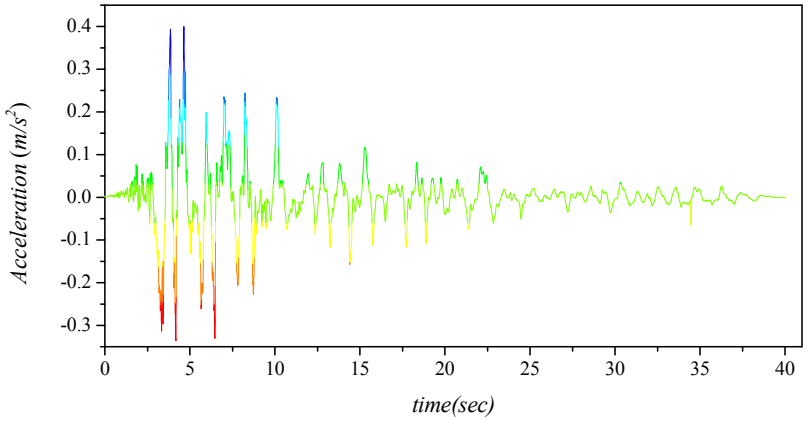

(b)

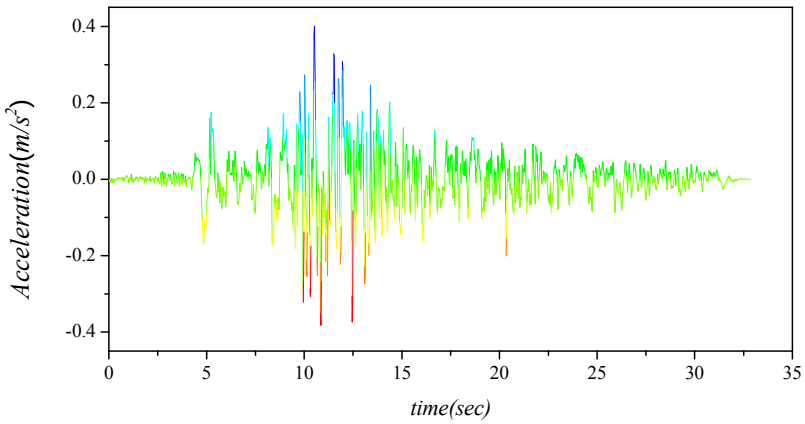

(c)

Fig. 3 (a) Acceleration recorded during Tabas the near field earthquake (PGA = 0.4 g); (b) Acceleration recorded during Northridge near field earthquake (PGA = 0.4 g); (c) Acceleration recorded during Imperial Valley near field earthquake (PGA = 0.4 g)

Table 1 Unsealed earthquake records used for non-linear analysis (Bayat *et al*. 2011b)

	Near field		
Earthquake	Imperial Valley 1979/10/15	Northridge 1994/01/17	Tabas, Iran 1978/09/16
Magnitude	M(6.5)Ml(6.6)Ms(6.9)	M(6.7)Ml(6.6)Ms(6.7)	M(7.4)Ml(7.7)Ms(7.4)
Station	952 El Centro	74 Sylmar-Converter Sta	9101 Tabas
Data source	USGS	DWP	--------
PGA	0.519	0.612	0.836
Distance (Km)	Closest to fault rapture (1.0)	Closest to fault rapture (6.2)	Hypocentral (3.0)
Site condition	CWB(D1) USGS(C)	CWB(C) USGS(C)	CWB(C)

The ADAS devices dissipate the energy by possessing the stable hysteretic loops resulting from the yielding of steel plates.

The ductility ratio μ is

$$\mu = \frac{\delta_R}{\delta_y} \tag{3.2}$$

In Fig. 2, $K' = NK$. Substituting Eq. (3.2) into Eq. (3.1) leads to

$$F_R = K'\delta_y + aK'\left(\mu\delta_y - \delta_y\right) = K'\delta_y\left(1 + a\mu - a\right) = KN\delta_y\left(1 + a\mu - a\right) \tag{3.3}$$

The stiffness of a steel plate, K can be determined as (Pong *et al*. 2009)

$$K = \frac{2EBT^3}{3H^3}\left(X - \text{shape steel plate}\right) \tag{3.4}$$

4. Characteristics of the near field earthquake records

Three unscaled earthquake records were applied to structures for nonlinear dynamic analysis with different PGA's. Table 1 is a full detail of these records.

5. Nonlinear dynamic time history assumptions

In this paper, the SMRF buildings with ADAS devices are analyzed. Nonlinear time history analysis involves the computation of dynamic response at each time increment concerning due consideration given to the inelasticity in members. The Input energy and its terms are evaluated. The numerical simulations were carried out by PERFORM 3D.V4.

- The frames were designed prior to this study in accordance with Uniform Building Code 97 requirements, based upon the static analysis for the minimal base shear force. After designing of the SMRF buildings, the ADAS devices were assigned to the frames and designed for F_R in Eq. (3.1).

We consider the following criteria for this study:

- Soil type is assumed Sc (very dense soil and soft rock) according to UBC97 (1997) code.
- The *P*-Delta effect is included in the analysis.
- The non-linear behavior of models is assumed from FEMA273 (1997).
- The plastic hinges in analysis are assumed perfectly elastic-plastic.
- A 0.005s time step be used for all non-linear analysis of models.
- Strength loss is ignored in non-linear analysis of systems.
- The value of *a* in Eq. (3.1) = 0.12
- Poisson's ratio = 0.3
- Elastic modulus = 2.0×10^6 kPa
- Yield stress =2400 Kg/cm^2
- Damping ratio is: 5%
- The properties of dampers are shown in Table 2.
- Chevron bracing were designed to have elastic behavior during an earthquake. Therefore, the sections of the chevrons are IPB 340 for 5 and ten story buildings and IPB450 for 15 story buildings.

Table 2 The properties of dampers (Whittaker *et al*. 1989)

Type of the damper	The Geometric properties						
	H (cm)	b-top & bottom (cm)	B middle (cm)	*T* (cm)	Δy (cm)	*Py* (Kg)	*K* (Kg/cm)
ADAS	12.7	6.35	1.27	0.64	0.2794	306	1094

Table 3 The first mode period of 3 bays SMRF frames with ADAS devices

Type of system	Number of story		
	5 story	10 story	15 story
SMRF + ADAS	0.43 s	0.86 s	1.18 s

Table 4 Design sections for the 5 story structure

Storey	The left side columns	The left interior columns	The left span beams	The right interior columns	The middle span beams	The right side columns	The right span beams
1	IPE360	HE240-B	IPE360	HE280-B	IPE360	HE280-B	HE240-B
2	IPE400	HE240-B	IPE360	HE260-B	IPE400	HE260-B	HE240-B
3	IPE360	HE220-B	IPE360	HE240-B	IPE360	HE240-B	HE220-B
4	IPE330	HE200-B	IPE330	HE220-B	IPE330	HE220-B	HE200-B
5	IPE300	HE180-B	IPE300	HE160-B	IPE300	HE160-B	HE180-B

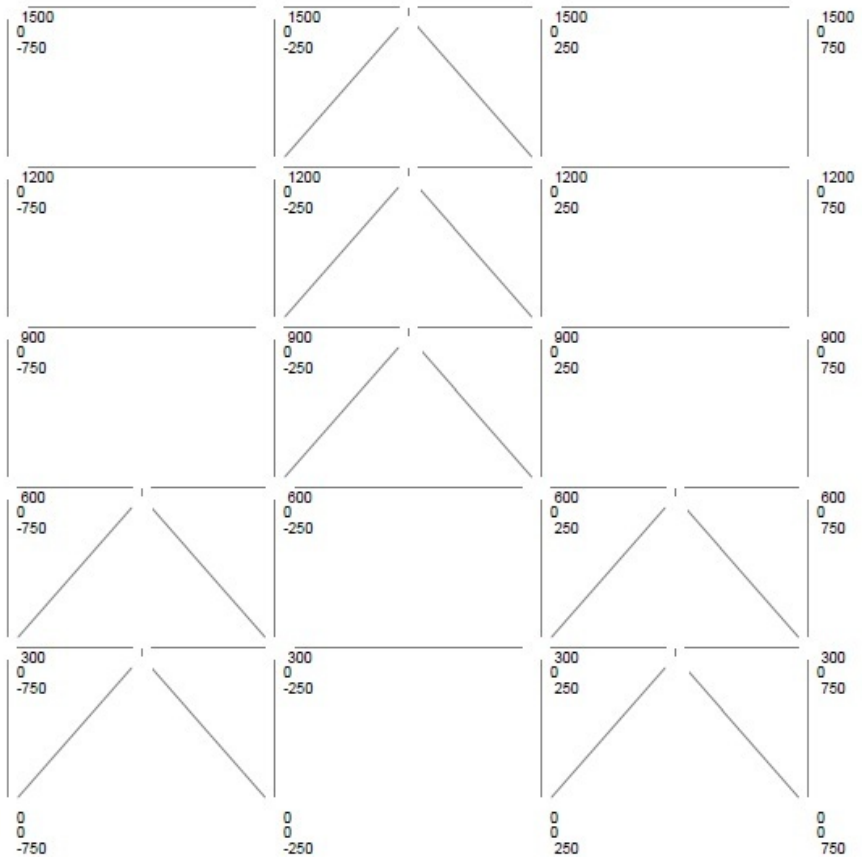

Fig. 4 Type of studied 5 story SMRF frame with ADAS devices in Perform 3D

Table 5 Design sections for the 10 story structure

Storey	The left side columns	The left interior columns	The left span beams	The right interior columns	The middle span beams	The right side columns	The right span beams
1	IPE400	HE300-B	IPE400	HE400-B	IPE400	HE400-B	HE300-B
2	IPE450	HE300-B	IPE450	HE320-B	IPE450	HE320-B	HE300-B
3	IPE450	HE280-B	IPE450	HE320-B	IPE450	HE320-B	HE280-B
4	IPE400	HE260-B	IPE450	HE300-B	IPE400	HE300-B	HE260-B
5	IPE400	HE260-B	IPE400	HE300-B	IPE400	HE300-B	HE260-B
6	IPE400	HE240-B	IPE400	HE280-B	IPE400	HE280-B	HE240-B
7	IPE400	HE220-B	IPE400	HE260-B	IPE400	HE260-B	HE220-B
8	IPE360	HE200-B	IPE360	HE240-B	IPE360	HE240-B	HE200-B
9	IPE330	HE200-B	IPE330	HE220-B	IPE330	HE220-B	HE200-B
10	IPE300	HE200-B	IPE300	HE180-B	IPE300	HE180-B	HE200-B

- Connection between beam and column can be realized as a hinge which is able to transmit only shear force (Whittaker *et al*. 1989).
- Tables 3 to5 show the design sections for the 5, 10 and 15 story structures.

The first periods of structures are as Table 3.

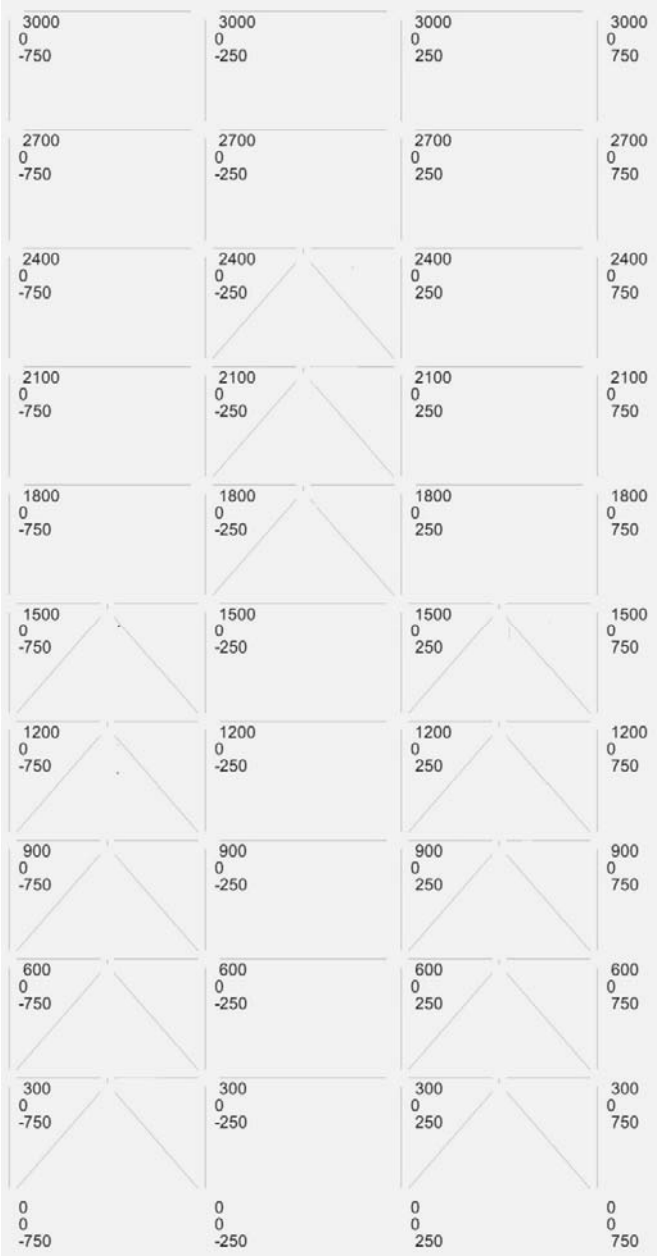

Fig. 5 Type of studied 10 story SMRF frame with ADAS devices in Perform 3D

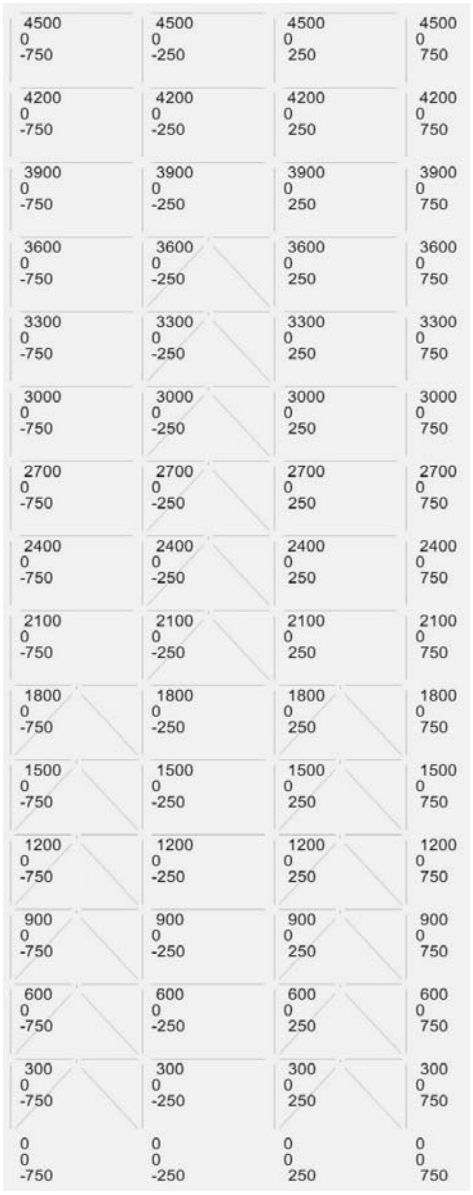

Fig. 6 Type of studied 15 story SMRF frame with ADAS devices in Perform 3D

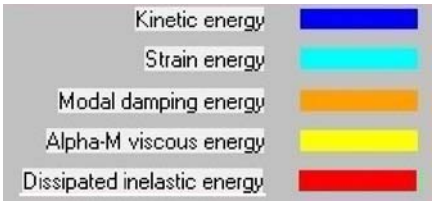

Fig. 7 Colors related to each energy

Table 6 Design sections for the 10 story structure

Storey	The left side columns	The left interior columns	The left span beams	The right interior columns	The middle span beams	The right side columns	The right span beams
1	IPE360	HE500-B	IPE360	HE550-B	IPE360	HE550-B	HE500-B
2	IPE450	HE400-B	IPE450	HE450-B	IPE450	HE450-B	HE400-B
3	IPE500	HE340-B	IPE450	HE450-B	IPE500	HE450-B	HE340-B
4	IPE450	HE340-B	IPE450	HE440-B	IPE450	HE440-B	HE340-B
5	IPE450	HE300-B	IPE450	HE400-B	IPE450	HE400-B	HE300-B
6	IPE450	HE300-B	IPE450	HE360-B	IPE450	HE360-B	HE300-B
7	IPE450	HE300-B	IPE450	HE340-B	IPE450	HE340-B	HE300-B
8	IPE450	HE280-B	IPE450	HE320-B	IPE450	HE320-B	HE280-B
9	IPE450	HE260-B	IPE400	HE300-B	IPE450	HE300-B	HE260-B
10	IPE400	HE260-B	IPE400	HE280-B	IPE400	HE280-B	HE260-B
11	IPE400	HE260-B	IPE400	HE260-B	IPE400	HE260-B	HE260-B
12	IPE360	HE240-B	IPE360	HE260-B	IPE360	HE260-B	HE240-B
13	IPE330	HE240-B	IPE360	HE260-B	IPE330	HE260-B	HE240-B
14	IPE330	HE220-B	IPE330	HE240-B	IPE330	HE240-B	HE220-B
15	IPE300	HE200-B	IPE300	HE180-B	IPE300	HE180-B	HE200-B

6. Results and discussions

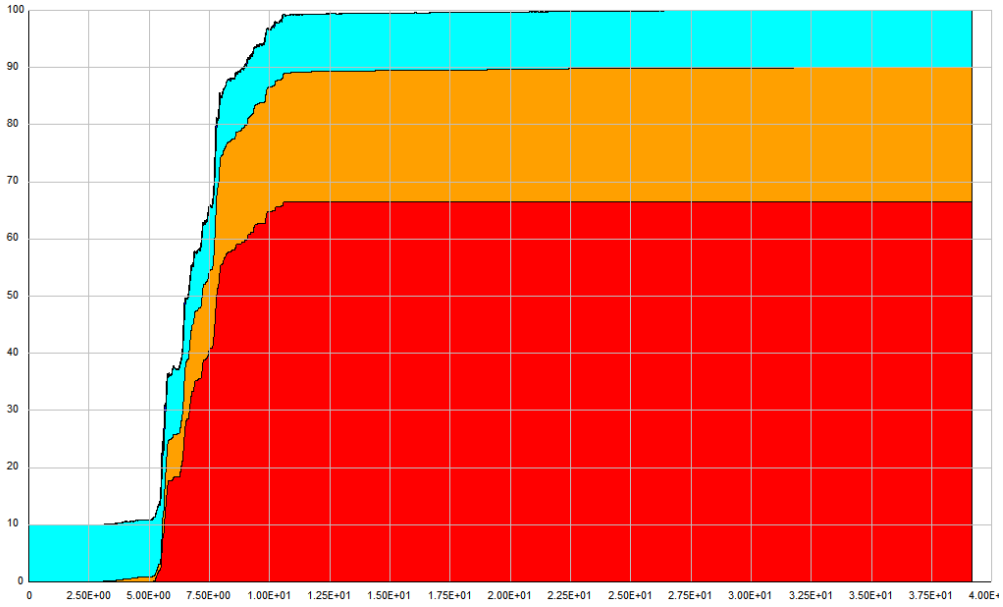

Fig. 8 Time history of Input energy to 5 story model under Imperial Valley with PGA = 0.4 g

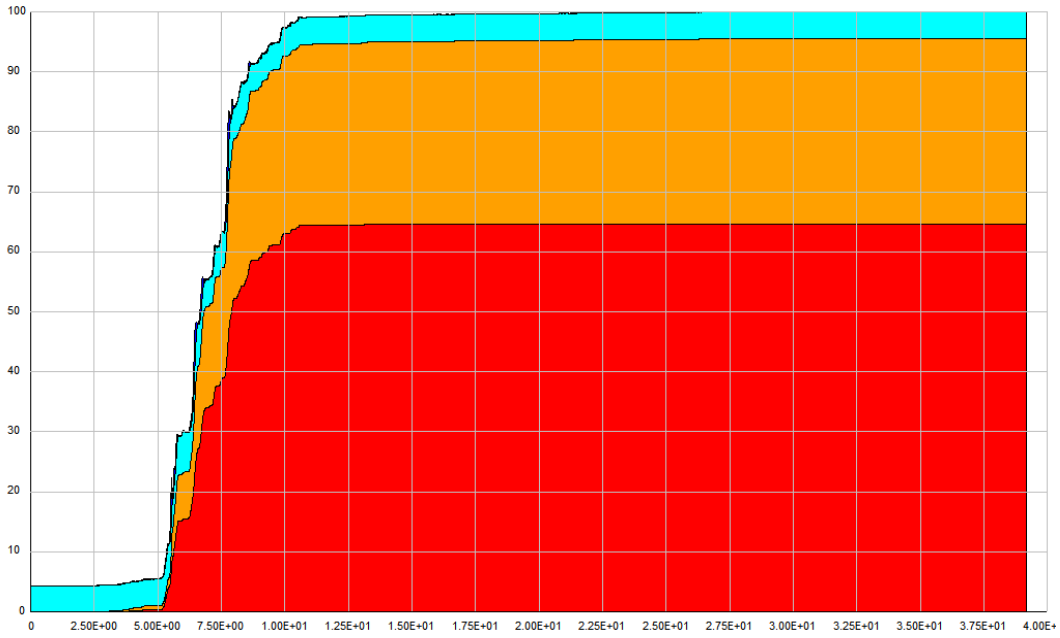

Fig. 9 Time history of Input energy to 5 story model under Imperial Valley with PGA = 0.6 cg

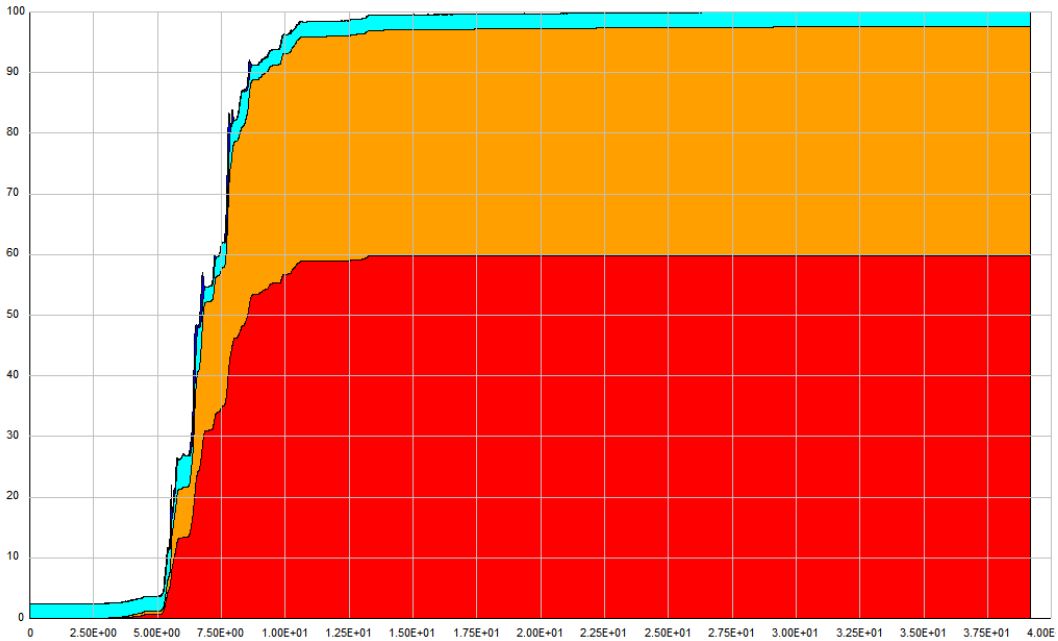

Fig. 10 Time history of Input energy to 5 story model under Imperial Valley record with PGA = 0.8 g

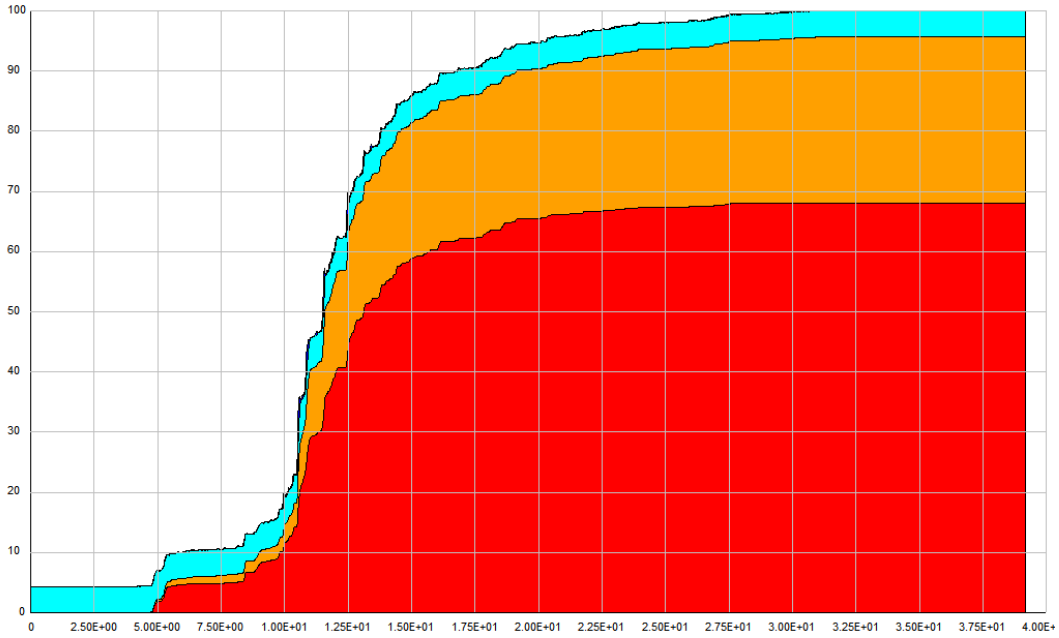

Fig. 11 Time history of Input energy to 5 story model under Tabas record with PGA = 0.4 g

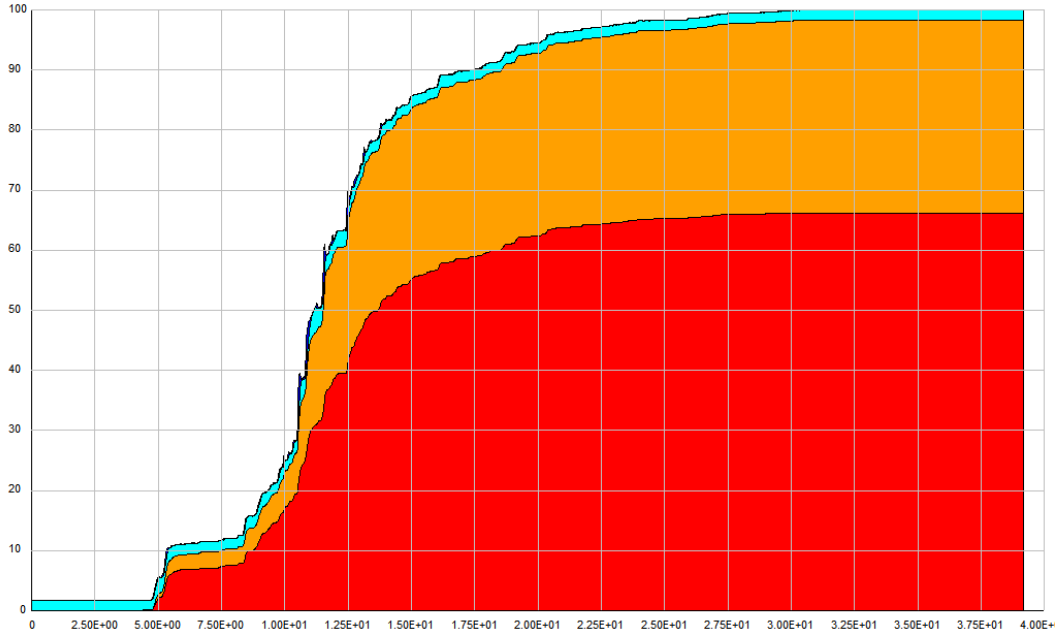

Fig. 12 Time history of Input energy to 5 story model under Tabas record with PGA = 0.6 g

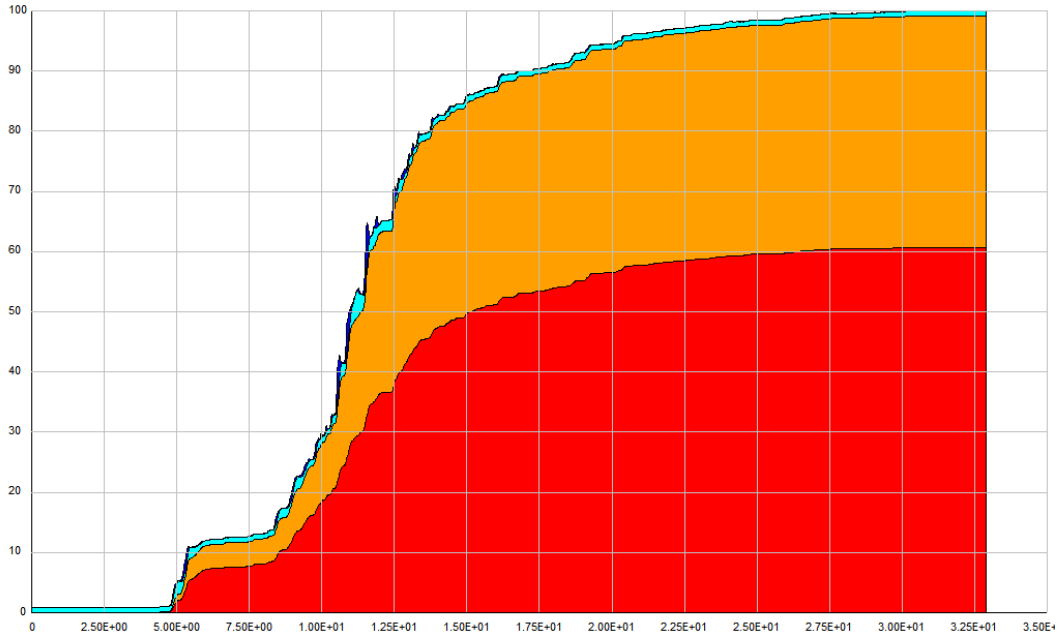

Fig. 13 Time history of Input energy to 5 story model under Tabas record with PGA = 0.8 g

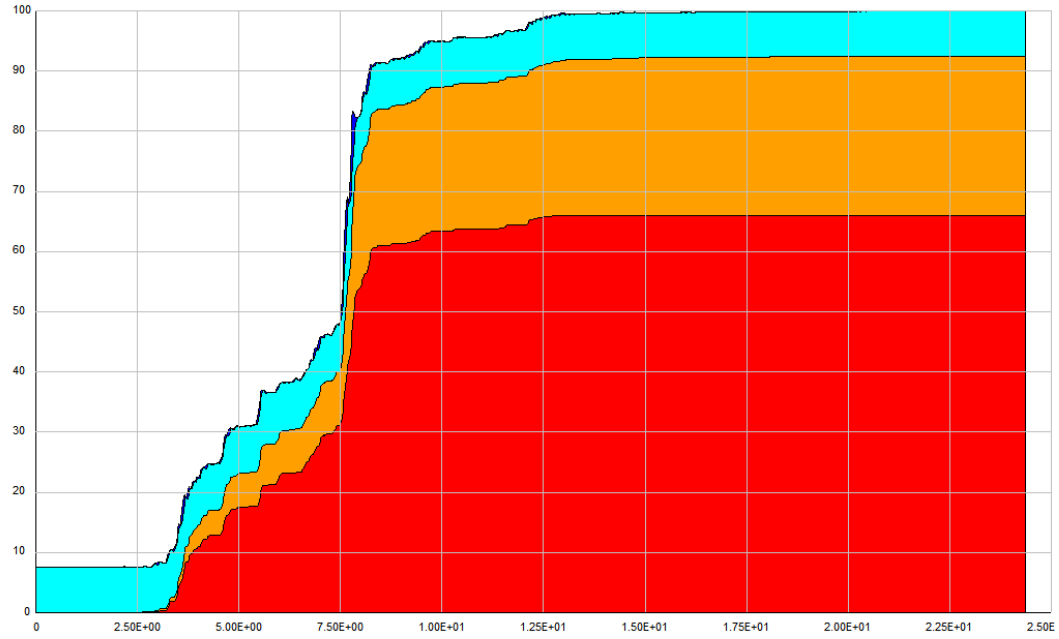

Fig. 14 Time history of Input energy to 5 story model under Northridge record with PGA = 0.4 g

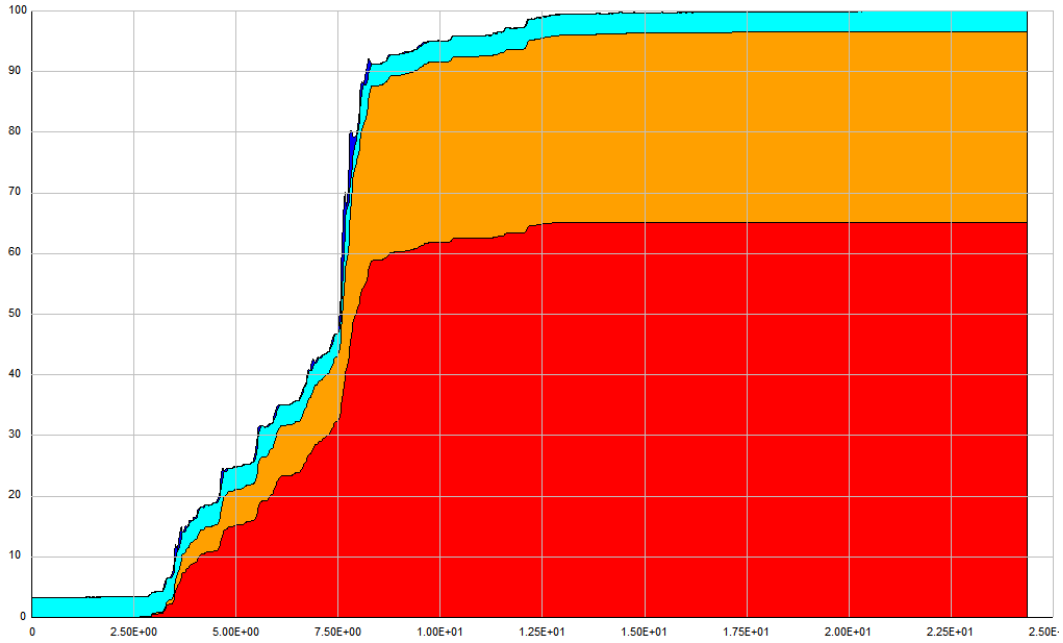

Fig. 15 Time history of Input energy to 5 story model under Northridge record with PGA = 0.6 g

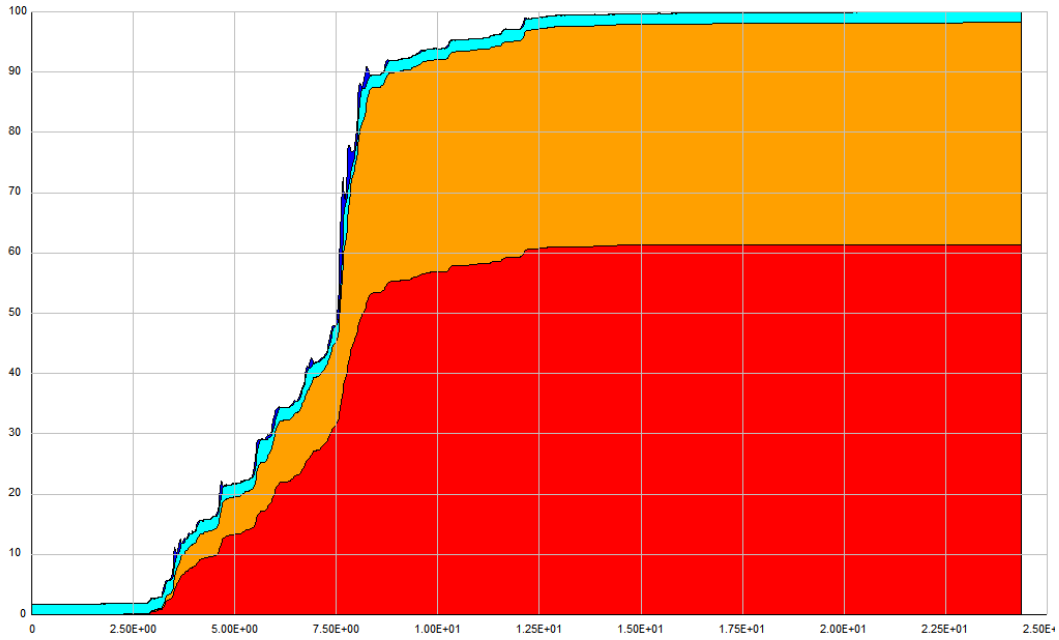

Fig. 16 Time history of Input energy to 5 story model under Northridge record with PGA = 0.8 g

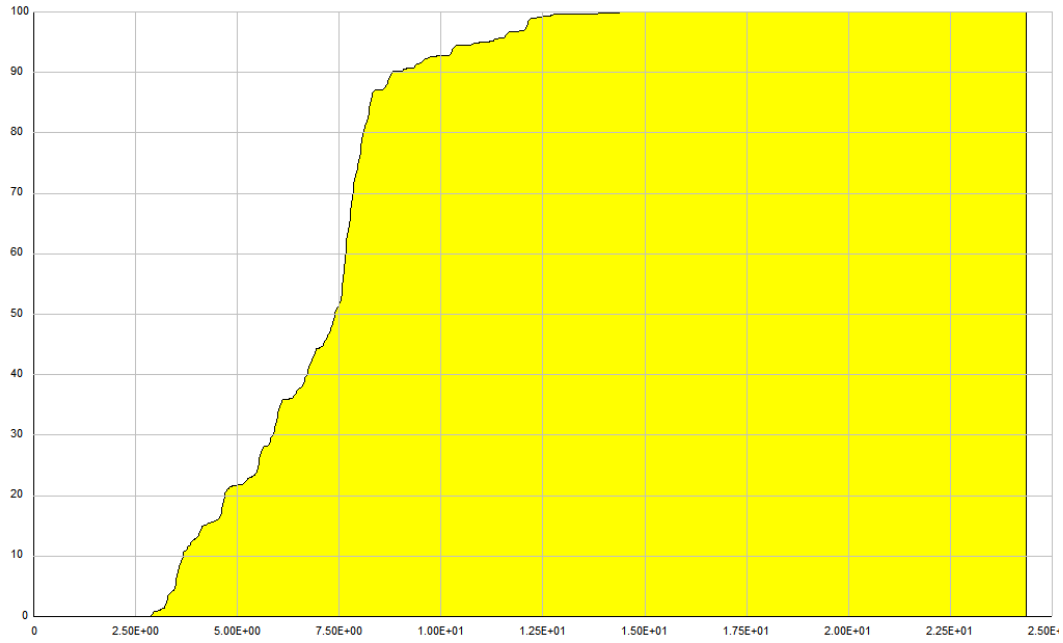

Fig. 17 Time history of Hystertic energy to 5 story model under Northridge record with PGA = 0.8 g

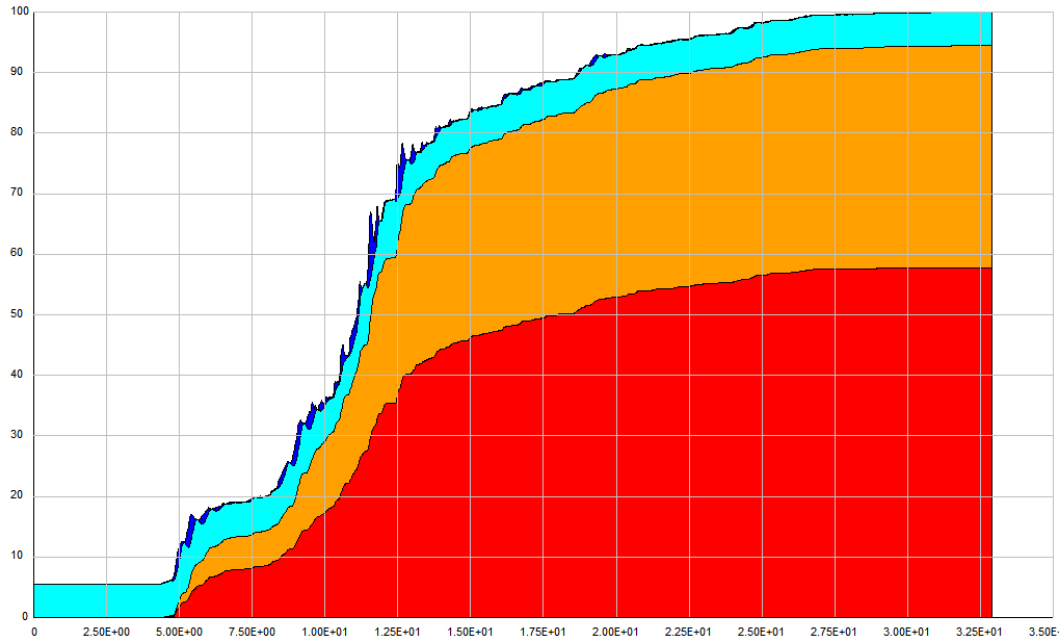

Fig. 18 Time history of Input energy to 10 story model under Tabas record with PGA = 0.4 g

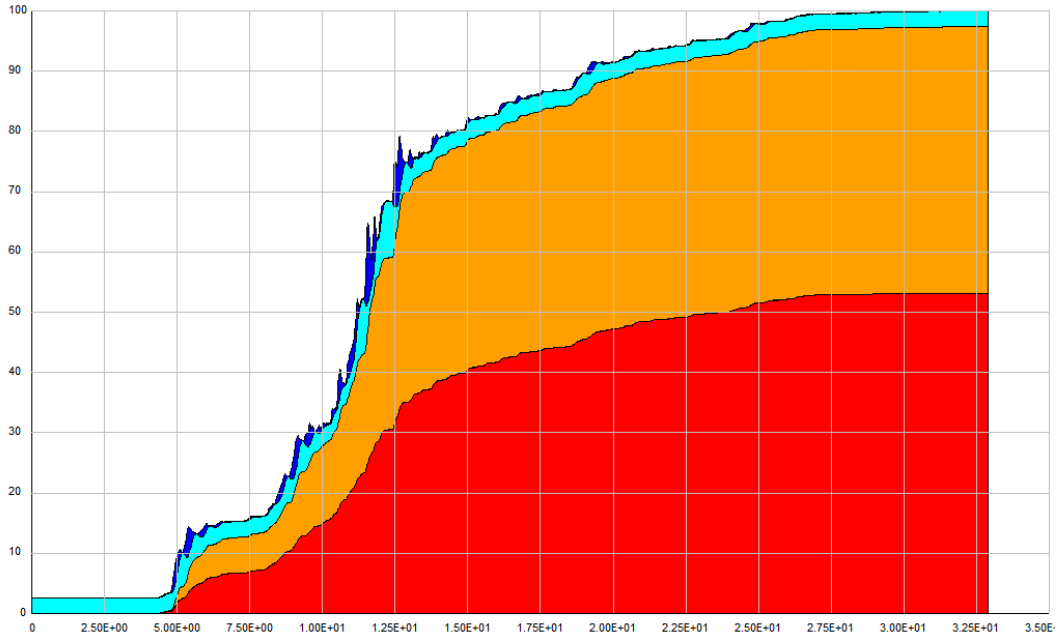

Fig. 19 Time history of Input energy to 10 story model under Tabas record with PGA = 0.6 g

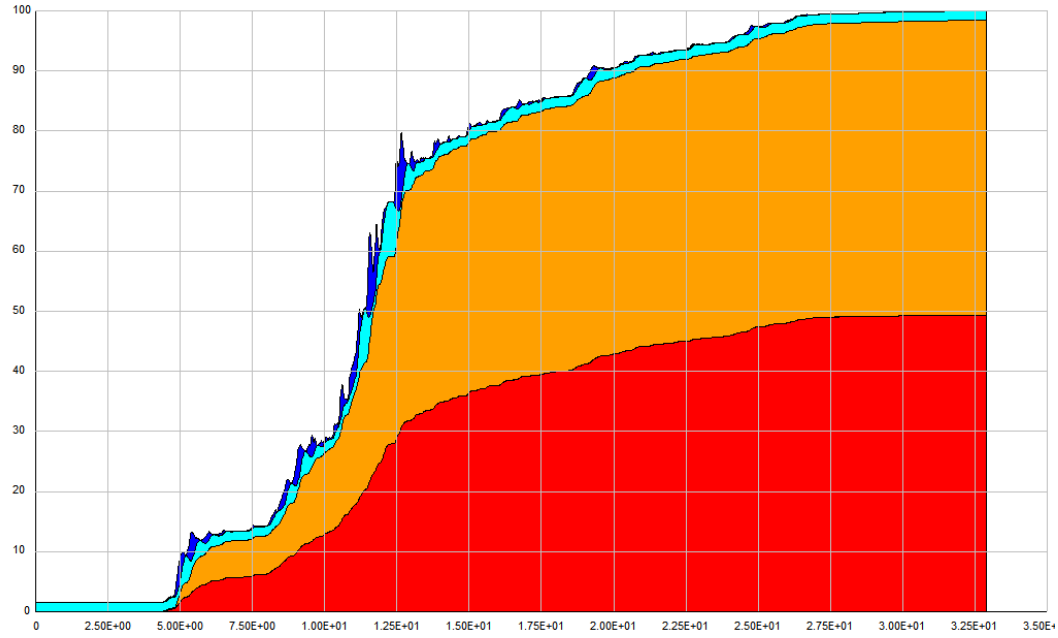

Fig. 20 Time history of Input energy to 10 story model under Tabas record with PGA = 0.8 g

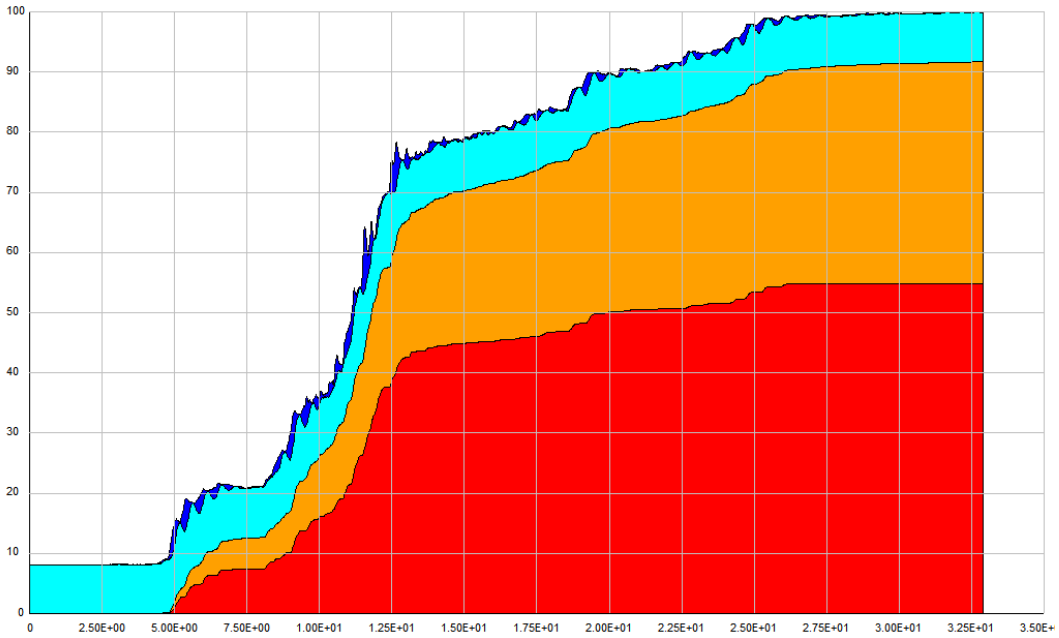

Fig. 21 Time history of Input energy to 15 story model under Tabas record with PGA = 0.4 g

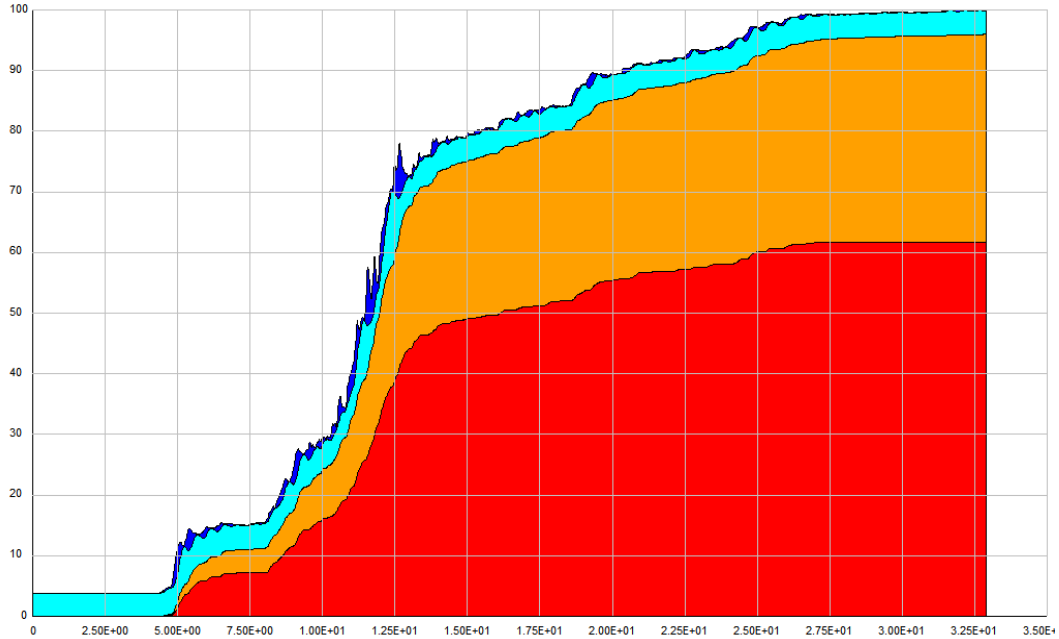

Fig. 22 Time history of Input energy to 15 story model under Tabas record with PGA = 0.6 g

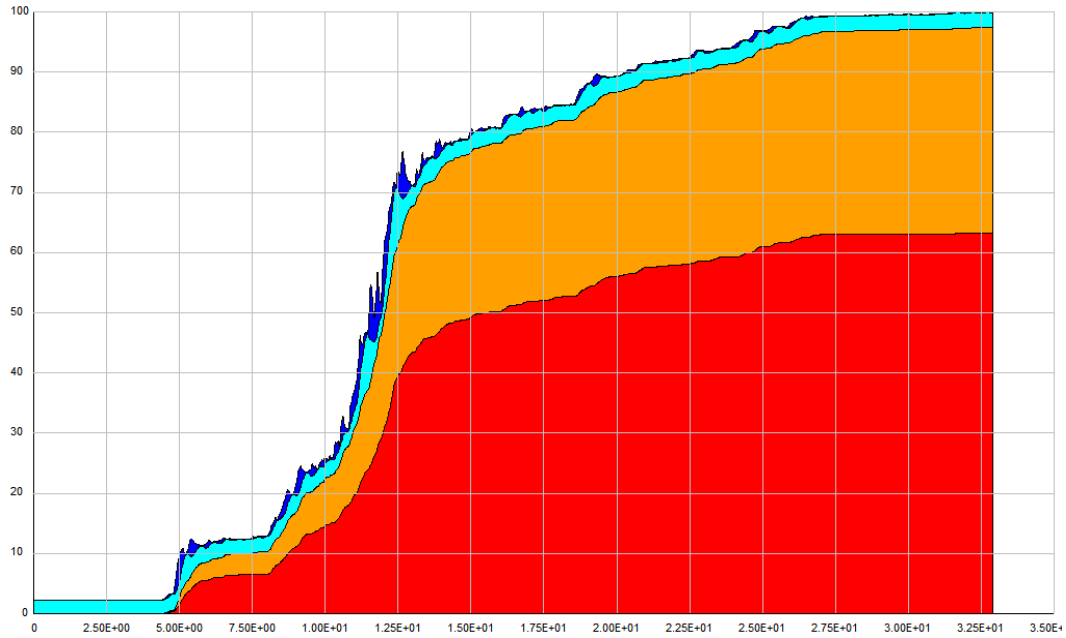

Fig. 23 Time history of Input energy to 15 story model under Tabas record with PGA = 0.8 g

By considering the Figs. 8 to 23, the typical scheme of the energy figures are same and the differences are just in their input energies. Table 7 shows the percentage of dissipated energy by the ADAS devices. The input energies are increased by increasing PGA.

When the input energy increases the strain energy is decreased in the structures and the damping energy is increased, too. The main considerable part is the amount of ADAS energy absorption.

Figs. 14 to 16, for the 10 story building are the same as the 5 story building. From the figures; it is obvious that the 50% of input energy has been absorbed by ADAS devices.

Hysteresis loops of ADAS devices are shown in Figs. 24 to 29 for the first floor and fifth floor of the structures to show that the lower stories have a larger shear force and the ADAS devices experience more deformations and yielding behavior than the upper floors.

The 15 story building has the longer period rather than the 5 and 10 story ones; therefore it's behavior is different. From Figs. 21 to 23, the strain energy is more than the 5 and 10 story buildings under the three different earthquakes and this amount is decreased by increasing the intensity of the earthquake motion. The behaviors of the structures during these earthquakes are similar. We have put the response of the structure under Tabas near fault ground motion for different PGA's. The structures are able to use their maximum damping capability in the high earthquake intensities. The above figures indicate the suitable behavior of ADAS devices under these different intensities. By increasing the height of structures, the period of the buildings are increased and the input energies are also increased, but the way of dividing these energies to different terms is the same as 5 and 10 story ones.

Table 7 The dissipated percentage of the ADAS elements under different earthquakes

Structures	Earthquakes	Input energy (kgf.cm)	Dissipated percentages by ADAS elements (%)
5 story	Tabas 0.4 g	0.740 e6	68
	Tabas 0.6 g	1.923 e6	66
	Tabas 0.8 g	3.809 e6	61
	Imperial Valley 0.4 g	0.327 e6	67
	Imperial Valley 0.6 g	0.752 e6	65
	Imperial Valley 0.8 g	1.381 e6	60
	Northridge 0.4 g	0.740 e6	66
	Northridge 0.6 g	0.998 e6	65
	Northridge 0.8 g	1.845 e6	61
10 story	Tabas 0.4 g	2.181 e6	58
	Tabas 0.6 g	4.732 e6	53
	Tabas 0.8 g	8.292 e 6	50
	Imperial Valley 0.4 g	0.928 e6	56
	Imperial Valley 0.6 g	2.035 e6	54
	Imperial Valley 0.8 g	3.610 e6	50
	Northridge 0.4 g	0.954 e6	57
	Northridge 0.6 g	1.938 e6	55
	Northridge 0.8 g	3.293 e6	56
15 story	Tabas 0.4 g	3.56 e6	55
	Tabas 0.6 g	7.647 e6	61
	Tabas 0.8 g	13.35 e6	63
	Imperial Valley 0.4 g	1.716 e6	53
	Imperial Valley 0.6 g	3.465 e6	55
	Imperial Valley 0.8 g	6.097 e6	60
	Northridge 0.4 g	1.682 e6	50
	Northridge 0.6 g	3.21 e6	56
	Northridge 0.8 g	5.222 e6	61

The ADAS devices greatly contribute to absorbing input energies from the near fault ground motions. For example, for a 5 story building under all the applied records, the hysteretic curve grows rapidly to reach its maximum amount. In this period of time, some members of structures are damaged when they entered to the nonlinear stage. In all structures the maximum part of input energy is dissipated by ADAS elements. The damping energy is helping to absorb input energy after a short time from the beginning of the earthquake and starts with a rapid slope to damp the input energy. The damping energy has a great effect in reduction of earthquake structural damage. The amount of input energy to structures and it's dissipation of it, could present the performance of structures during the earthquake.

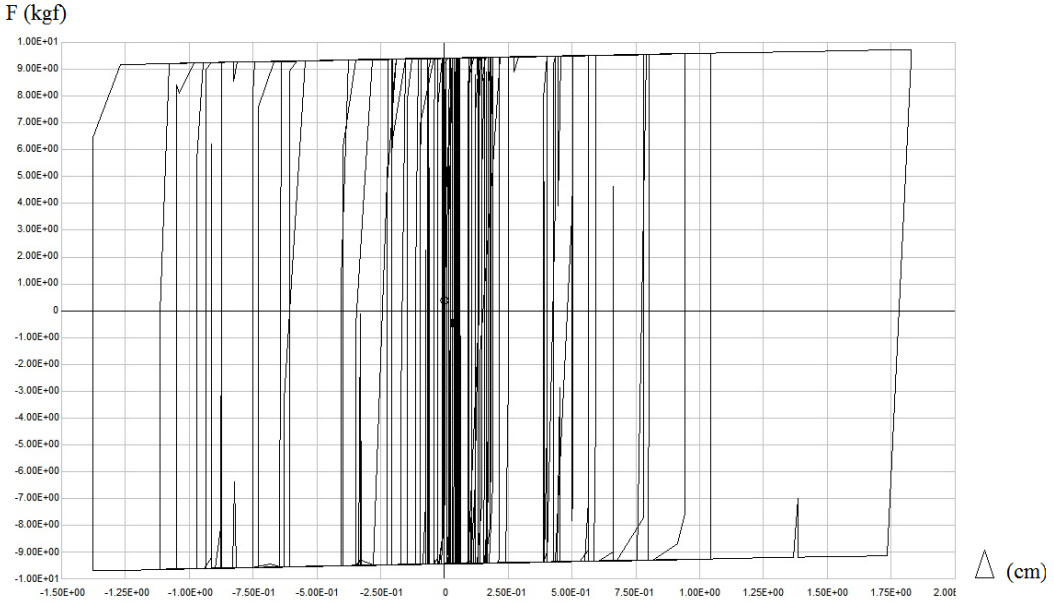

Fig. 24 Hysteresis loops of ADAS devices of 5 story building- first floor under Tabas record with PGA = 0.8 g

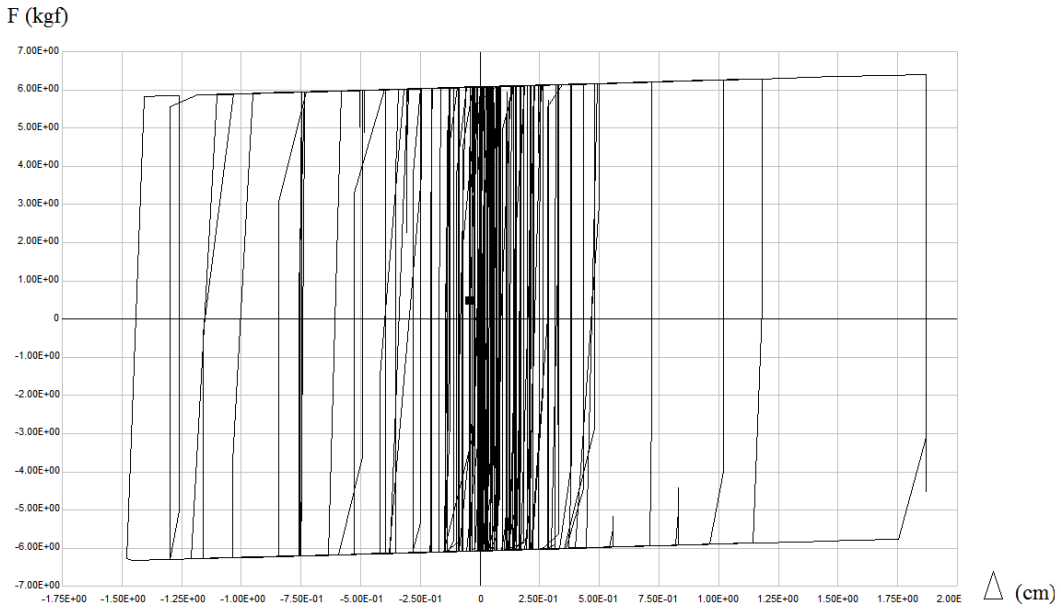

Fig. 25 Hysteresis loops of ADAS devices of 5 story building - fifth floor under Tabas record with PGA = 0.8 g

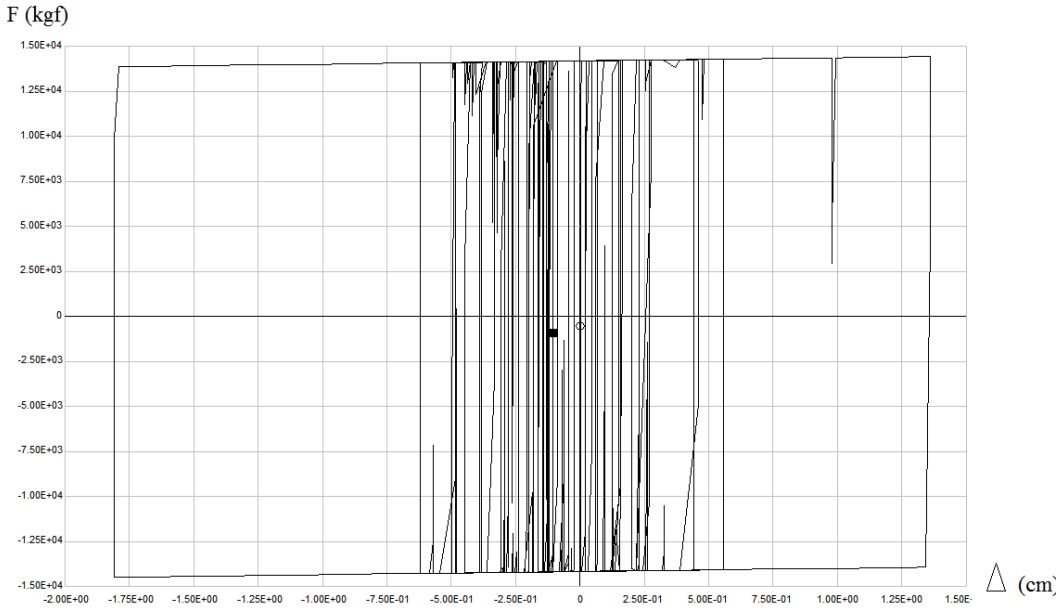

Fig. 26 Hysteresis loops of ADAS devices of 10 story building - first floor under Tabas record with PGA = 0.8 g

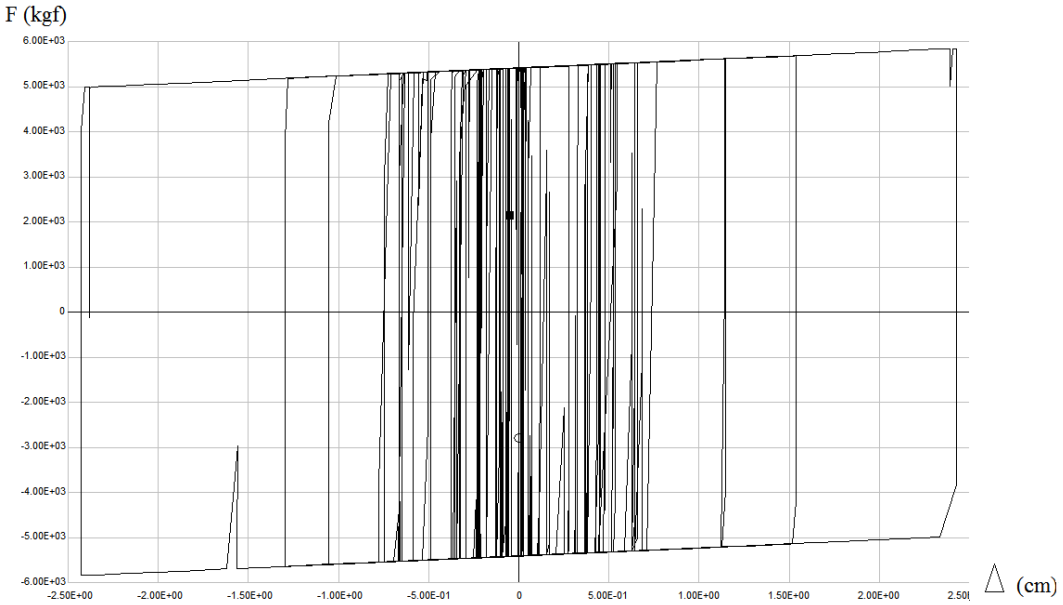

Fig. 27 Hysteresis loops of ADAS devices of 10 story building - fifth floor under Tabas record with PGA = 0.8 g

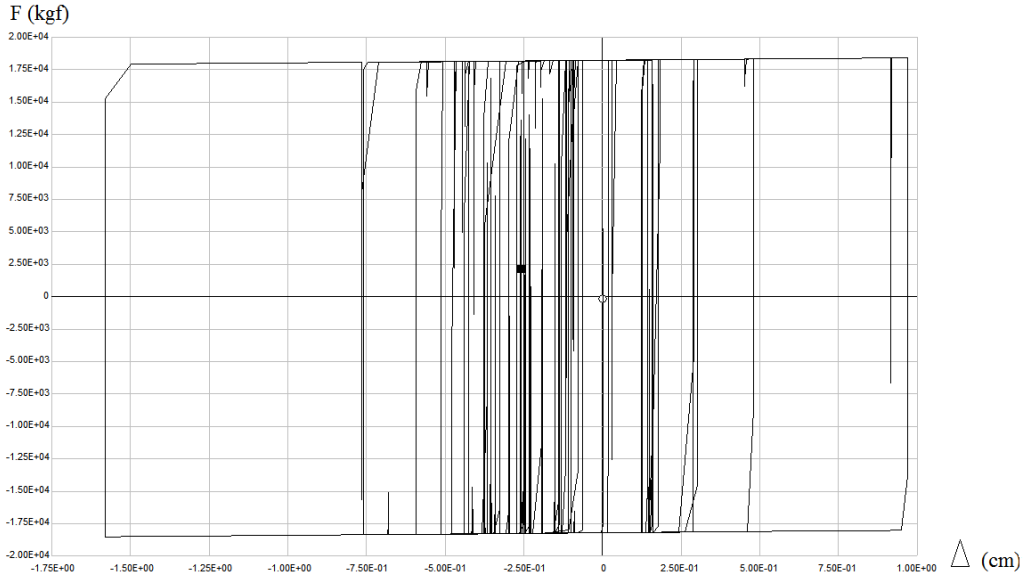

Fig. 28 Hysteresis loops of ADAS devices of 15 story building - first floor under Tabas record with PGA = 0.8 g

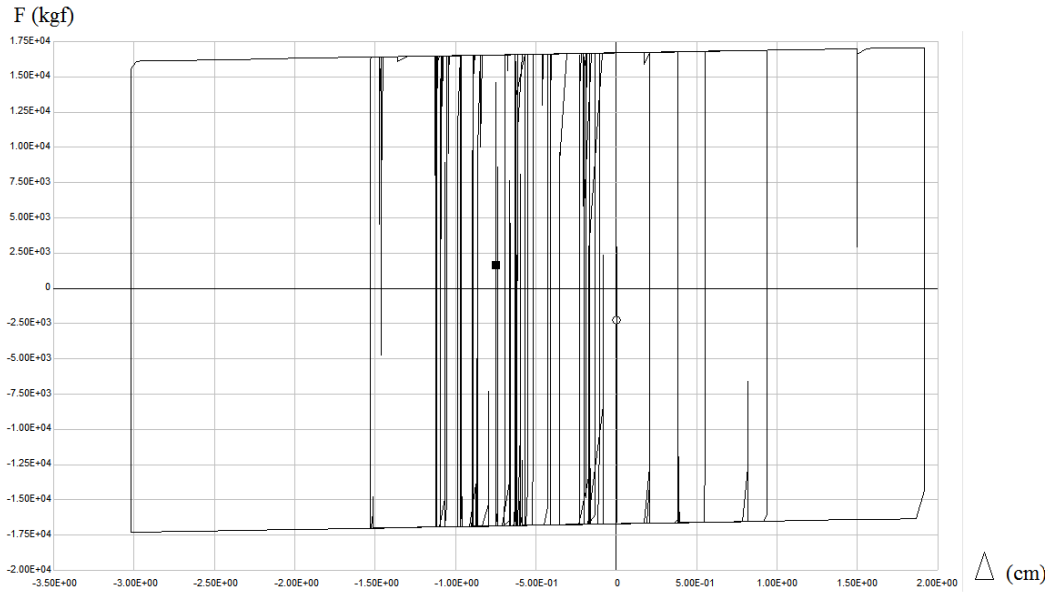

Fig. 29 Hysteresis loops of ADAS devices of 15 story building - fifth floor under Tabas record with PGA = 0.8 g

The input energy contains 4 terms: some of it dissipated by damping of structures and nonlinear behavior of structural elements and the others absorbs as strain energy and kinetic energy.

$$E_i = E_k + E_\xi + E_s + E_h \tag{6.1}$$

Eq. (1.6) is the structure equilibrium energy equation. E_i is the input energy of an earthquake, E_k is the kinetic energy, E_ξ is the damping energy, E_s is the elastic strain energy and the E_h is the hysteretic energy.

In the structures equipped with energy dissipating devices we had identified the appropriate locations for the placement of the first plastic hinges. First place is the ADAS elements which absorbs the hysteretic energy of the earthquake. All the analysis demonstrate the amount of hysteretic energy in ADAS elements is more than 50% and that shows the great performance of these elements during the near fault ground motions.

7. Conclusions

In this paper we have investigated the behavior of SMRF frames with yielding dampers under the selected near fault ground motions. The usage of the ADAS system by absorbing more input energy with a high ratio of hysteretic to input energy has a better seismic performance under the near fault ground motions. The Tabas, Imperial valley and Northridge earthquakes with different PGA's were applied to structures (0.4 g, 0.6 g, 0.8 g). The increasing or decreasing of PGA has no effect on the typical scheme of the input energy in different systems; the increasing of PGA just increases the differences of the input energies. By considering the height of a building on the input energy and plastic energy in the ADAS systems, we conclude that the behavior structures during the near fault ground motions are different and depending on the frequency content and the characteristic of the structure especially the height. In the structures located in the near fault regions, by increasing the numbers of stories, the period of the structure is increased. The ADAS system gives a higher ratio of hysteretic to input energy and increases the seismic performance of structures during the near fault ground motions.

References

Aguirre, M. and Sánchez, A.R. (1992), "Structural seismic damper", *J. Struct. Eng.*, *ASCE*, **118**(5), 1158-1171.

Apostolakis, G. and Dargush, G. (2010), "Optimal seismic design of moment resisting steel frames with hysteretic passive devices", *Earthq. Eng. Struct. Dyn.*, **39**(4), 355-376.

Baker, J.W. (2007), "Quantitative classification of near-fault ground motions using wavelet analysis", Bulletin of the Seismological Society of America, **97**(5), 1486-1501.

Barrón, R. and Ayala, A.G. (2013), *An Energy-Based Design Method for Buildings with Supplemental Damping and Nonlinear Behavior*, Seismic Behaviour and Design of Irregular and Complex Civil Structures, Springer, 297-307.

Bayat, M. and Abdollahzadeh, G.R. (2011a), "Analysis of the steel braced frames equipped with ADAS devices under the far field records", Latin American Journal of Solids and Structures, **8**(2), 163-181.

Bayat, M. and Abdollahzadeh, G.R. (2011b), "On the effect of the near field records on the steel braced frames equipped with energy dissipating devices", Latin American Journal of Solids and Structures, **8**(4),

429-443.
Bergman, D.M. and Goel, S.C. (1987), "Evaluation of cyclic testing of steel-plate device for added dampingand stiffness", University of Michigan, Ann Arbor, MI, USA.
Brown, P., Aiken, I.D. and Jafarzadeh, F.J. (2001), *Seismic Retrofit of the Wallace F. Bennett Federal Building*, Modern Steel Construction, AISC, Chicago, IL, USA.
Constantinou, M.C. and Symans, M.D. (1993), "Seismic response of structures with supplemental damping", *Struct. Des. Tall Build.*, **2**(2), 77-92.
Erfani, S., Babazadeh Naseri, A. and Akrami, V. (2012), "The beneficial effects of beam web opening in Seismic behavior of steel moment frames", *Steel Compos. Struct., Int. J.*, **13**(1), 35-46.
FEMA 273 (1997), NEHRP Guidelines and Commentary for the Seismic Rehabilitation of Buildings, Report FEMA 273 (Guidelines), Federal Emergency Management Agency, Washington, D.C., USA.
Kelly, J.M., Skinner, R.I. and Heine, A.J. (1972), "Mechanisms of energy absorption in special devices for use in earthquake resistant structures", Bulletin of New Zealand National Society for Earthquake Engineering, **5**(3), 63-88.
Longo, A., Montuori, R. and Piluso, V. (2012a), "Theory of plastic mechanism control of dissipative truss moment frames", *Eng. Struct.*, **37**, 63-75.
Longo, A., Montuori, R. and Piluso, V. (2012b), "Failure mode control and seismic response of dissipative truss moment frames", *J. Struct. Eng.*, **138**(11), 1388-1397.
Martinez-Romero, E. (1993), "Experiences on the use of supplemental energy dissipators on building structures", *Earthq. Spectra*, **9**(3), 581-624.
Monti, M.D. and Robinson, W.H. (1996), "A lead shear damper suitable for reducing the motion induced by earthquake and wind", *Eleventh Worm Conference on Earthquake Engineering*.
Moreschi, L.M. (2000), "Seismic design of energy dissipation systems for optimal structural performance", Ph.D. Thesis, Virginia Polytechnic Institute and State University, Blacksburg, VA, USA.
Parulekar, Y., Reddy, G., Vaze, K., Ghosh, A., Kushwaha, H. and Babu, R.R. (2009), "Seismic response analysis of RCC structure with yielding dampers using linearization techniques", *Nucl. Eng. Des.*, **239**(12), 3054-3061.
PERFORM 3D.V4, Analysis software, RAM International, L.L.C., University of California.
Pong, W., Lee, Z., Tsai, C.S. and Chen, B.J. (2009), "Heuristic design procedure for structures with displacement dependent damping devices", *Eng. Comput.*, **26**(4), 347-359.
Ponzo, F.C., Di Cesare, A., Nigro, D., Vulcano, A., Mazza, F., Dolce, M. and Moroni, C. (2012), "JET-PACS project: Dynamic experimental tests and numerical results obtained for a steel frame equipped with hysteretic damped chevron braces", *J. Earthq. Eng.*, **16**(5), 662-685.
Rai, D.C., Annam, P.K. and Pradhan, T. (2013), "Seismic testing of steel braced frames with aluminum shear yielding dampers", *Eng. Struct.*, **46**, 737-747.
Reyes-Salazar, A., Soto-Lopeza, M.E., Bojorquez-Mora, E. and Lopez-Barraza, A. (2012), "Effect of modeling assumptions on the Seismic behavior of steel buildings with perimeter moment frames", *Struct. Eng. Mech., Int. J.*, **41**(2), 183-204.
Shih, M.H. and Sung, W.P. (2005), "A model for hysteretic behavior of rhombic low yield strength steel added damping and stiffness", *Comput. Struct.*, **83**(12-13), 895-908.
Skinner, R.I., Kelly, J.M. and Heine, A.J. (1975), "Hysteresis dampers for earthquake resistant structures", *Earthq. Eng. Struct. Dyn.*, **3**(3), 287-296.
Symans, M.D., Charney, F.A., Whittaker, A.S., Constantinou, M.C., Kircher, C.A., Johnson, M.W. and McNamara, R.J. (2008), "Energy dissipation systems for seismic applications: Current practice and recent developments", *J. Struct. Eng.*, **134**(1), 0733-9445.
Whittaker, A.S., Bertero, V.V., Alonso, L.J. and Thompson, C.L. (1989), "Earthquake simulator testing of steel plate added damping and stiffness elements", Report UCB/EERC-89/02, University of California, Berkeley, CA, USA.
Whittaker, A.S., Bertero, V.V., Thompson, C.L. and Alonso, L.J. (1991), "Seismic testing of steel plate energy dissipation devices", *Earthq. Spectra*, **7**(4), 563-604.
Uniform Building Code (1997).

Zahrai, S.M. and Jalali, M. (2014), "Experimental and analytical investigations on Seismic behavior of ductile steel knee braced frames", *Steel Compos*. *Struct*., *Int*. *J*., **16**(1), 1-21.

CC

Nomenclature

u	=	relative displacement of the mass with respect to the ground,
u_g	=	earthquake ground displacement.
E_I	=	Input energy
E_k	=	Kinetic energy;
E_D	=	Damping energy
E_A	=	Composed of recoverable elastic strain energy and irrecoverable hysteretic energy.
a	=	an unknown coefficient to be determined from the experimental data
K'	=	elastic stiffness of the ADAS devices
δ_R	=	maximum relative displacement
δ_y	=	yield displacement of the ADAS devices
E	=	elastic modulus of steel
B	=	base width
T	=	Thickness
H	=	height of the steel plates
K	=	stiffness of a steel plate
N	=	number of steel plates